Clays and Clay Minerals, Vol. 29, No. 3, 184–190, 1981.

GEOCHEMISTRY AND MINERALOGY OF AN UNUSUAL DIABASE SAPROLITE NEAR COLUMBIA, SOUTH CAROLINA

L. R. GARDNER, I. KHEORUENROMNE[1], AND H. S. CHEN

Department of Geology, University of South Carolina, Columbia, South Carolina 29208

Abstract—Empirical reaction progress diagrams showing the trends of major element oxide concentrations (in g/cm³) as functions of bulk density for a diabase saprolite reveal discontinuities in the trends of Al_2O_3, MgO, H_2O+, and nonextractable Fe_2O_3. The discontinuities coincide with discontinuities in the trends of (1) the kaolinite-smectite 001 peak-intensity ratio, (2) the smectite 002-001 peak intensity ratio, and (3) the smectite basal spacing as functions of bulk density. The discontinuities are apparently related to redox conditions in the weathering profile because they occur at a depth where siderite veins first appear in the saprolite. Oxidizing conditions in the upper part of the profile appear to have favored the formation of Fe-rich smectite over kaolinite, whereas reducing conditions deeper in the profile favored the formation of kaolinite over Al-rich smectite. These results indicate that where geochemical conditions favor retention of Fe over Al, smectites can form in preference to kaolinite or gibbsite even under conditions of strong leaching.

Key Words—Bulk density, Diabase, Kaolinite, Oxidation, Saprolite, Smectite, Weathering.

INTRODUCTION

Gardner *et al.* (1978) described the geochemistry and clay mineralogy of a granite saprolite near Columbia, South Carolina, and showed that if the saprolite formed by isovolumetric chemical weathering (Millot and Bonifas, 1955), its chemical analyses can be cast in the form of an empirical reaction progress diagram (Helgeson *et al.*, 1969). In this type of diagram the volumetric concentrations (in g/cm³) of the various oxides are plotted against bulk density, the overall reaction progress variable. Such diagrams are useful because theoretical reaction paths can be plotted on them and thus provide a means of testing the validity of postulated weathering reactions. The present paper describes the volumetric geochemistry and clay mineralogy of a diabase saprolite that cuts the earlier studied granite saprolite as a dike (Figure 1). The reaction progress diagram for this saprolite and its clay mineralogy indicate that its formation involved a complex history of oxidation and reduction.

SITE DESCRIPTION

The saprolite is exposed in a granite quarry in Cayce, South Carolina, (N33°58.09′, W81°03.07′) owned by the Martin Marietta Corporation. As shown in Figure 1, the granite is cut by a diabase dike about 7 m thick. The upper 10–15 m of both the granite and diabase have been altered to saprolite in which the crystalline texture of the parent rocks is clearly visible. The saprolite is overlain by a thin veneer (~4 m) of Coastal Plain sediment of unknown but probable Tertiary age (personal communication, D. J. Colquhoun, Department of Geology, University of South Carolina, Columbia, S.C.). The granite saprolite normally has a bleached white appearance, but near the diabase it is pale green. The white and green saprolite are separated by a zone of reddish-brown granite saprolite (Figure 1).

The fresh diabase is dark grey to black and consists of 1–2-mm size grains. The mineralogy of the diabase is unusual in that it contains substantial amounts of talc and chlorite in addition to plagioclase and pyroxene. The fresh rock is also cut by numerous joints that are filled with 1–2-cm veins of dark green, fibrous to platy smectite. In the lower part of the diabase saprolite these smectite veins are largely replaced by siderite (Gardner and Kheoruenromne, 1980) which forms a crusty boxwork pattern. Neither the fresh diabase nor the diabase saprolite in joint blocks between the siderite veins contain siderite. The upper 2 m of the saprolite is also free of siderite veins, although the relict joint pattern is outlined by thin planar zones of iron oxide-stained saprolite.

METHODS OF STUDY

Saprolite samples were collected along a nearly vertical profile through the center of the dike (Figure 1) by hammering a metal cylinder (5-cm inner diameter) into freshly exposed saprolite so that the volume of each sample could be determined from the geometry of the cylinder. The bulk density (Table 1) of each sample was determined from the measured volume and the sample weight after drying at 105°C for 24 hr. The concentration of major elements was determined by atomic absorption spectrophotometry on acid-digested samples (Medlin *et al.*, 1969). FeO was determined by titration

[1] Present address: Department of Soils, Kasetsart University, Bangkok-9, Thailand.

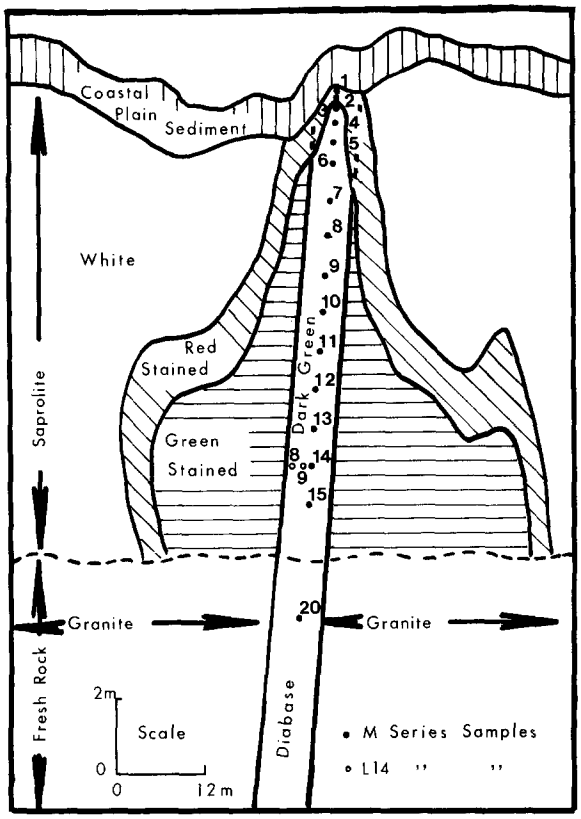

Figure 1. Sketch of saprolite exposed in uppermost bench of granite saprolite quarry, Cayce, South Carolina. Fresh granite and diabase are exposed in cuts on lower benches.

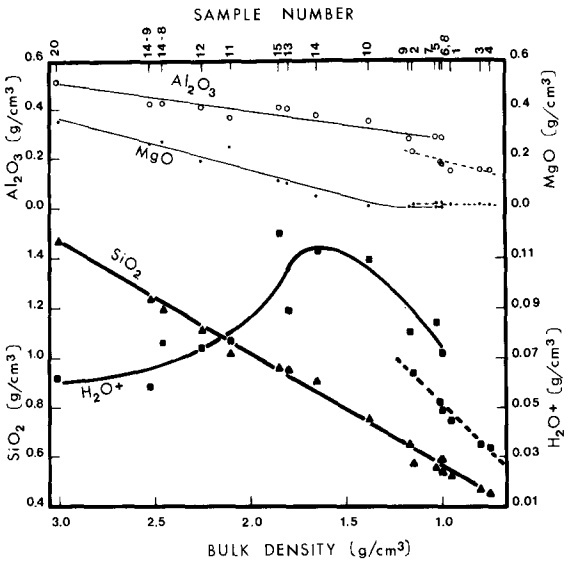

Figure 2. Variation of SiO_2, Al_2O_3, MgO, and H_2O+ with bulk density. Dashed lines represent trends offset above discontinuity.

with a standard dichromate solution with diphenylamine sulfonic acid as the indicator (Shapiro and Brannock, 1962). Extractable iron oxide was determined by a modified sodium dithionite-citrate-bicarbonate method (Jackson, 1965). The loss of weight after ignition at 810°C was used as an estimate of the structural water content. The clay mineralogy of the saprolite was de-

Table 1. Chemical analyses of diabase saprolite.[1]

Sample	Depth	Bulk density (g/cm³)	SiO_2 (%)	Al_2O_3 (%)	Fe_2O_3B (%)	Fe_2O_3E (%)	FeO (%)	MgO (%)	CaO (%)	Na_2O (%)	K_2O (%)	TiO_2 (%)	P_2O_5 (%)	H_2O+ (%)	Total (%)
M1	0.10	0.96	54.63	15.78	16.19	4.04	0.00	1.82	0.98	—	0.36	0.66	0.02	4.69	99.17
M2	0.25	1.15	49.86	20.07	12.96	5.83	0.01	1.31	0.82	—	0.50	0.67	0.05	5.58	97.66
M3	0.50	0.80	58.57	19.25	10.75	0.13	0.06	2.22	1.02	0.03	0.71	0.88	0.06	4.43	98.11
M4	1.00	0.75	60.76	19.45	12.29	0.10	0.09	1.61	0.78	—	0.58	0.52	0.14	4.53	100.85
M5	1.50	1.01	58.86	17.85	12.04	0.19	0.08	1.98	1.14	—	0.33	0.64	0.16	5.17	98.44
M6	2.00	1.00	59.30	17.52	11.27	0.24	0.08	2.01	1.01	—	1.16	0.58	0.16	4.88	98.21
M7	3.00	1.03	53.95	27.79	5.27	0.19	0.14	0.58	0.80	—	0.34	0.77	0.15	8.28	98.26
M8	4.00	1.00	54.22	28.16	6.45	0.16	0.16	0.88	0.80	—	0.36	0.78	0.12	7.21	99.30
M9	5.00	1.17	55.82	23.75	6.57	0.27	0.10	0.97	0.83	—	0.46	0.81	0.10	6.92	96.78
M10	6.00	1.38	54.93	25.16	7.40	0.50	2.46	1.00	1.24	—	0.48	0.76	0.11	7.92[2]	101.96
M11	7.00	2.11	48.31	17.16	6.75	0.49	4.15	11.94	7.05	1.09	0.37	0.55	0.19	3.65	101.70
M12	8.00	2.26	49.38	18.23	7.89	0.92	3.80	8.60	7.16	1.33	0.43	0.56	0.20	3.29	101.79
M13	9.00	1.81	52.72	22.24	8.52	0.61	2.21	5.51	3.97	0.97	0.42	0.72	0.15	4.94	102.98
M14	10.00	1.66	54.53	22.81	9.56	0.64	1.24	2.69	1.16	0.02	0.56	0.85	0.11	6.80	100.97
M15	11.00	1.85	51.78	21.94	10.09	0.71	2.18	5.84	1.42	0.01	0.56	0.73	0.09	6.48	101.83
M20	30.00	3.01	48.68	17.09	3.13	0.37	6.26	11.84	10.43	1.40	0.32	0.48	0.25	2.06	102.31
L14-8	10.00	2.46	48.56	17.32	6.87	0.89	3.39	10.96	8.92	1.27	0.37	0.57	0.18	3.08	102.38
L14-9	10.00	2.52	49.11	16.85	5.95	1.14	3.98	10.47	9.53	1.36	0.39	0.58	0.21	2.33	101.90

[1] Based on oven-dried (110°C) samples. Dashes indicate oxides not detected. Fe_2O_3B = bound Fe_2O_3; Fe_2O_3E = extractable Fe_2O_3.

[2] Sample M10 contains 1.95% CO_2 which is included in H_2O+. All other samples contain <0.1% CO_2.

https://doi.org/10.1346/CCMN.1981.0290303 Published online by Cambridge University Press

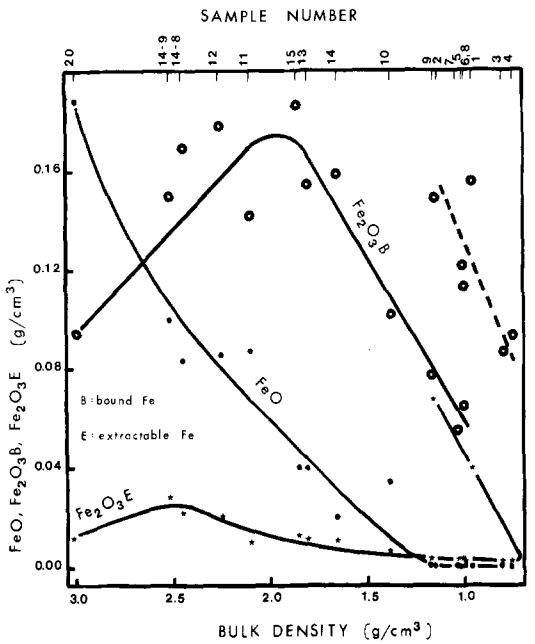

Figure 3. Variation of FeO and Fe_2O_3 with bulk density. Dashed lines represent trends offset above discontinuity.

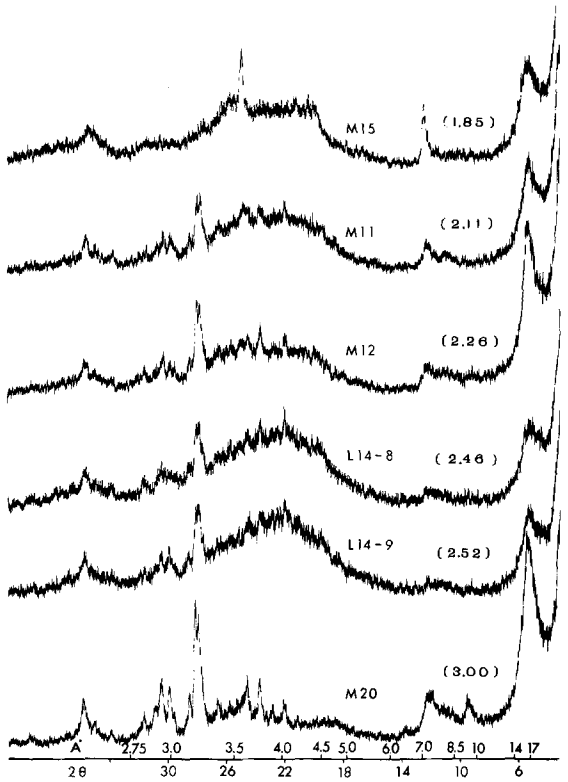

Figure 4. X-ray powder diffraction patterns arranged in order of bulk density. Numbers in brackets are bulk density values of samples. CuKα radiation, 35 Kv, 18 mA, range 10^3 counts/sec, 1-sec time constant, ethylene glycol treated.

termine by X-ray powder diffraction (XRD) (CuKα radiation) of clay + fine silt (<5 μm) suspensions from pulverized samples sedimented onto glass slides. All of the samples were X-rayed before and after saturation with ethylene glycol. Several samples were also X-rayed after various heat treatments. Modal analysis of the fresh diabase was obtained by point counting a thin section.

RESULTS

The weight-based concentration data and sample bulk densities are presented in Table 1. The weight-based concentration data were converted to volumetric concentrations (g/cm^3) by multiplying the weight-based concentrations (H_2O-free basis) by their corresponding bulk densities. The empirical reaction progress diagrams shown in Figures 2 and 3 were obtained by plotting the volumetric concentrations for each oxide against bulk density. The XRD patterns of ethylene glycol-saturated samples in Figures 4–6 are arranged in order of sample bulk densities, in rough accordance with their depth below the saprolite–sediment contact (Figure 1). Figure 7 summarizes the XRD data of Figures 4–6 and shows the variation of the kaolinite-smectite peak area ratios, the smectite 002-001 peak area ratios, and the spacing of the smectite 001 reflection as functions of bulk density. The smectite 001 values in Figure 7 are the averages of all the basal smectite reflections shown on individual patterns. Modal analysis of the fresh diabase indicates that it consists of 40% plagioclase, 29% clinopyroxene, 20% talc, 8% chlorite, and 2% opaque minerals.

The most outstanding feature of the data shown in Figures 2–7 is the discontinuity that exists between the six samples (M1–M6) from the upper two meters of saprolite and those below. The six upper samples occur in the zone where siderite veins are absent. Geochemically the discontinuity is revealed by the reaction progress paths of Al_2O_3, H_2O+, bound Fe_2O_3, and, to a lesser extent, MgO (Figures 2–3). In the lower samples the amount of Al_2O_3 decreases towards the surface in a linear fashion from 0.51 g/cm^3 at bulk density 3.0 g/cm^3 to about 0.28 g/cm^3 at bulk density 1.0 g/cm^3. The Al_2O_3 trend for the upper samples is also linear but is offset abruptly downward by about 0.05 g/cm^3 and declines with a slope about twice as steep as that of the former trend. Thus, it appears that the transition from the lower saprolite with siderite veins to the upper siderite-free saprolite is marked by an abrupt loss in Al_2O_3 and H_2O+ and that the rate of removal of Al_2O_3 was greater in the siderite-free saprolite. The abrupt loss of Al_2O_3 at this transition is compensated by an abrupt gain of bound (nonextractable) Fe_2O_3 in the upper saprolite. Most of this nonextractable iron presumably is in the structure of silicate minerals. There is an abrupt but small gain in MgO as well; however, the trends of

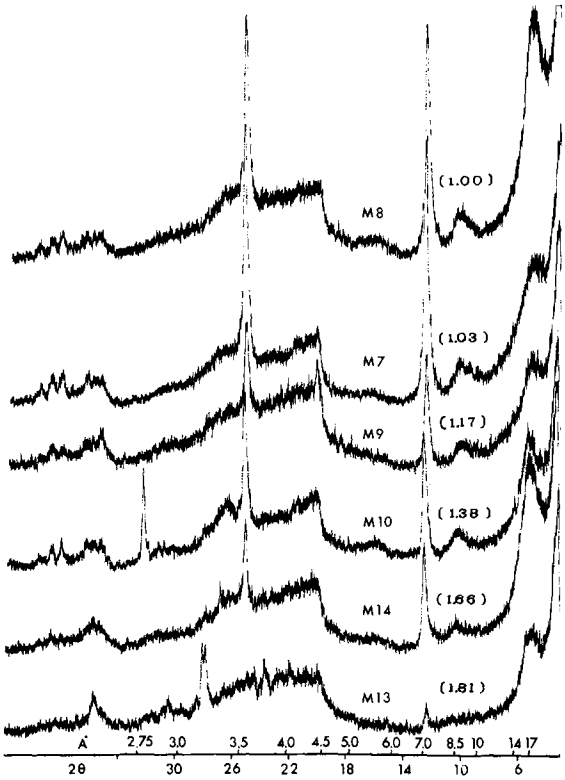

Figure 5. X-ray powder diffraction patterns arranged in order of bulk density. Numbers in brackets are bulk density values of samples. CuKα radiation, 35 kV, 18 mA, range 10^3 counts/sec, 1-sec time constant, ethylene glycol treated.

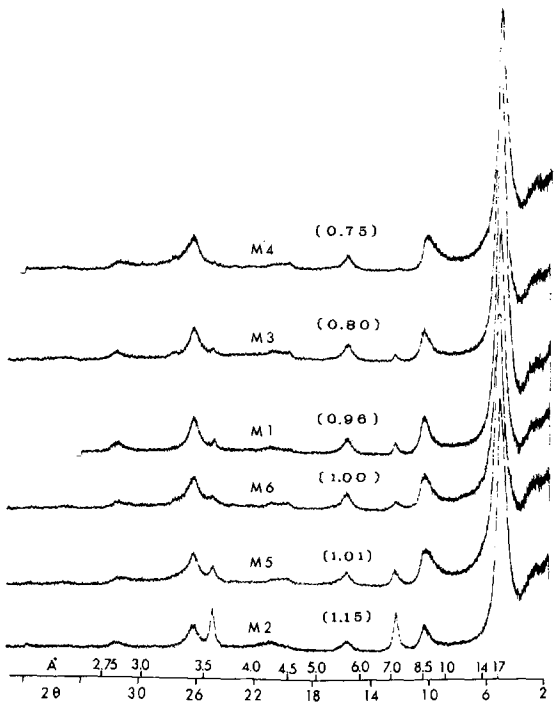

Figure 6. X-ray powder diffraction patterns arranged in order of bulk density. Numbers in brackets are bulk density values of samples. CuKα radiation, 35 kV, 18 mA, range 5×10^3 counts/sec, 0.5-sec time constant, ethylene glycol treated. Note change in range and time constant required to keep smectite peak on scale.

none of the other oxides appear to be offset by this transition.

Mineralogically the transition is marked by three discontinuities, as shown on Figure 7. In the saprolite below the transition the ratio of kaolinite to smectite progressively increases with decreasing bulk density. At the transition there is an abrupt decrease in this ratio. Above the transition the kaolinite:smectite ratio decreases, rather than increases, with decreasing bulk density (see inset, Figure 7). The second mineralogical discontinuity involves the peak-area intensity ratio of the smectite 002 and 001 reflections. This ratio is essentially zero in the deeper, nearly fresh samples, but at a bulk density of about 1.8 g/cm^3 it increases dramatically to the discontinuity. At the discontinuity the ratio abruptly drops from about 0.5 to 0.1. Above the discontinuity it again increases with decreasing bulk density but at a slower rate. Finally, the basal spacing of the smectite shows a noteworthy change at the transition. Below the transition the smectite basal spacing progressively increases from about 16.2 Å in the fresh rock to about 17.6 Å at the transition. Above the transition the basal spacing remains essentially constant at about 17.0 ± 0.05 Å.

DISCUSSION AND INTERPRETATION

The various discontinuities described above can not be explained simply as a result of the abrupt dilation of the saprolite that might have been caused by dissolution of siderite veins in the upper saprolite. Dilation would have caused decreases in all of the oxides and can not explain the increases in MgO and bound Fe_2O_3 or the mineralogical discontinuities. Likewise, illuviation of kaolinite from the upper saprolite is not a satisfactory explanation because this process can account for neither the discontinuity in bound Fe_2O_3 nor the lack of offset in the SiO_2 trend. Instead, the association of geochemical and mineralogical discontinuities with the disappearance of siderite in the upper saprolite suggests that the discontinuities are related to an abrupt change in the redox conditions in the profile.

In formulating additional hypotheses for the origin of the saprolite several observations should be kept in mind. First, abrupt redox boundaries in soil profiles commonly coincide with the position of the water table. Second, the position of a redox boundary may shift vertically as a result of water table fluctuations or the downward migration of an oxidizing weathering front. Third, reducing conditions occur when the dissolved oxygen in soil water is exhausted by the oxidation of

https://doi.org/10.1346/CCMN.1981.0290303 Published online by Cambridge University Press

organic matter, ferrous iron, and/or reduced sulfur. Finally the time of origin of the saprolite could either precede or follow deposition of the Coastal Plain sediment (Figure 1).

In deep residual soils Fe- and/or Al-rich crusts or hardpans commonly form at the capillary fringe of a water table. No such crust is evident in the saprolite. Also, relatively silica-rich clays tend to form below the water table because ground water is usually richer in SiO_2 than water draining the overlying vadose zone. In the saprolite the reverse relationship was observed as smectite dominates in the upper zone whereas kaolinite is more abundant in the lower zone. Finally if a water table existed at the discontinuity in the diabase saprolite one might expect it to extend more or less horizontally into the adjacent granite saprolite. This expectation does not conform well with the shape of the greenish and reddish halos in the adjacent granite saprolite (Figure 1). The draped aspect of the halos suggests that reducing conditions were confined to the vicinity of the diabase dike. Thus, it is unlikely that the discontinuity marks the position of a water table.

Instead, localization of reducing conditions near the dike suggests that removal of dissolved oxygen from the soil water resulted from the oxidation of some of the ferrous iron in the parent diabase. Concurrent hydrolysis reactions would have released some of the remaining ferrous iron into solution and increased the soil water pH which, in the presence of high subsurface CO_2 pressure, would have resulted in high concentrations of CO_3^{2-}. Such a sequence of reactions could have led to the precipitation of siderite veins. It is conceivable that these reactions took place after burial of the fresh diabase by Coastal Plain sediment, perhaps in a swamp or floodplain environment. In this case the entire weathering profile probably would have developed below a Coastal Plain water table over a long period of pervasive reducing conditions. If this were so, it is not clear why the siderite should be restricted to veins in the diabase saprolite. Furthermore, the reddish, oxidized, outer portion of the halo is difficult to reconcile with the idea that the entire weathering profile developed under reducing conditions. Indeed, the configuration of the halo suggests that the entire profile developed above the water table, the draped aspect of the halo probably resulting from the downward movement and outward dispersion of soil water enriched in iron and magnesium from the dike.

In any case further hypotheses on the history of the saprolite depends on whether one postulates that the siderite veins were once present in the upper saprolite. If so, the discontinuity may be related to the downward migration of oxidizing, acidic conditions wherein siderite dissolves according to the following reaction:

$$FeCO_3 + 3H^+ + \frac{1}{4}O_2 \rightarrow Fe^{+3} + CO_2 + 1\frac{1}{2}H_2O.$$

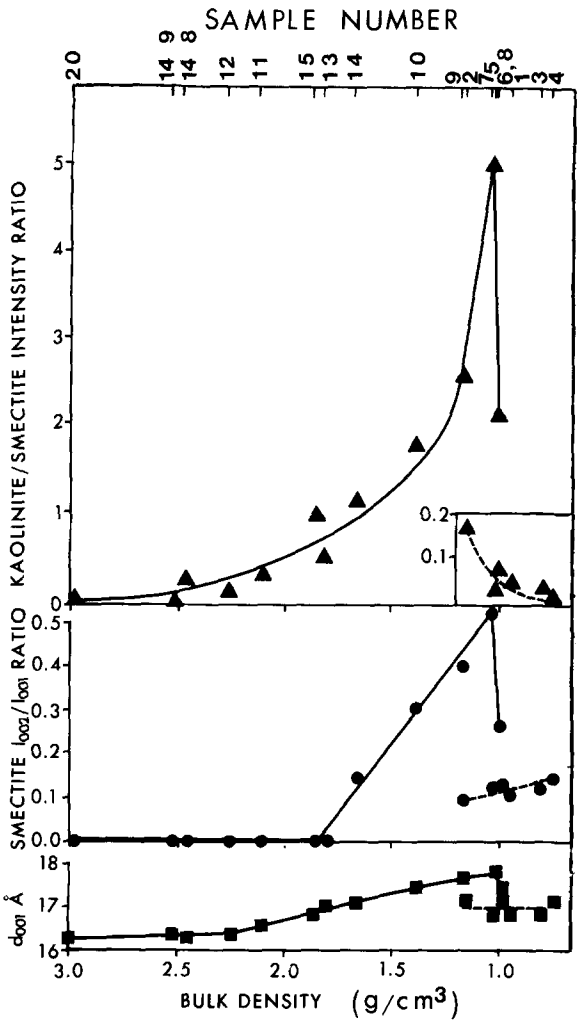

Figure 7. Variation of X-ray diffraction parameters with bulk density. Dashed lines represent trends offset above discontinuity.

Fe^{+3} thus produced could react with Al-rich smectite and/or kaolinite to form Fe-rich smectite at the discontinuity. Alternatively, if one assumes that oxidizing conditions prevailed in the upper saprolite since the onset of weathering, then presumably siderite never formed there at all. In this case the discontinuity may simply be a reflection of the lesser mobility of iron under oxidizing conditions so that the formation of Fe-rich smectite was favored in the upper saprolite. One difficulty with this hypothesis is that the white granite saprolite, which presumably formed under similar oxidizing conditions because it lies outside the reducing halo, has been thoroughly leached of iron (Gardner *et al.*, 1978) suggesting that conditions were fairly acidic or that the soil water contained complexing agents. If this is so, one might ask why the iron in the oxidized diabase saprolite was not also thoroughly leached. The answer

https://doi.org/10.1346/CCMN.1981.0290303 Published online by Cambridge University Press

is that the diabase contains substantially more iron than granite and contains minerals that tend to hydrolyze strongly, thus producing a more alkaline soil which promotes retention of iron.

Above the discontinuity further weathering resulted in an additional decrease in kaolinite such that at bulk density 0.75 g/cm³ kaolinite is not detectable by XRD (Figure 6, sample M4). Weathering in the upper saprolite is also marked by decreasing trends in Al_2O_3 and bound Fe_2O_3 (Figures 2 and 3). Partitioning calculations which distribute the volumetric concentrations of the oxides among kaolinite and smectite and estimate the structural formula of the smectite on the basis of mass- and charge-balance equations indicate a reduction in the kaolinite content from 0.0013 moles/cm³ at bulk density 1.15 g/cm³ (sample M2) to zero at bulk density 0.75 g/cm³ (sample M4). Over this reduction in bulk density the smectite content remains constant at about 0.0022 moles/cm³ but the ratio of Al to Fe in the octahedral layer of the smectite increases from 1.3 to 2.3.

In the deeper, less weathered portion of the saprolite the complex chemistry of the parent minerals in the diabase makes detailed interpretation of the XRD and chemical data difficult. Nevertheless these data indicate that weathering of the diabase in the zone below the redox discontinuity can be divided into two stages. The boundary between the stages occurs at a bulk density of about 1.8 g/cm³ at which point the smectite 002-001 intensity ratio begins to rise dramatically, the smectite basal spacing reaches 17.0 Å (Figure 7), and H_2O+ and bound Fe_2O_3 reach their maximum concentrations (Figures 2 and 3). At this bulk density most of the original Na_2O, CaO, and MgO has been lost and there is no XRD evidence for the presence of plagioclase or pyroxene. Between bulk density 3.0 and 1.8 g/cm³, weathering is characterized by an initial rapid disappearance of chlorite (7.2 Å) and talc (cf. samples M-20 and L-14-9, Figure 6), the oxidation of FeO to bound Fe_2O_3, and the production of a relatively small amount of kaolinite. In this stage the original chlorite and talc and possibly some of the pyroxene and plagioclase were converted into some sort of mixed-layer chlorite/smectite. From bulk density 1.8 to 1.0 g/cm³ weathering is characterized by the loss of bound Fe_2O_3 and increases in the smectite 002:001 intensity ratio and the kaolinite:smectite ratio. Because little of the original plagioclase or pyroxene remains in samples with bulk densities less than 1.8 g/cm³, the increase in the kaolinite:smectite ratio and the loss of bound Fe_2O_3 indicate that some of the smectite was destroyed and/or transformed into kaolinite. Interestingly, this is in contrast to the loss of kaolinite that occurs in the siderite-free saprolite discussed above. Finally, the increase in the smectite 001 spacing to values greater than 17.0 Å and the dramatic increase in the smectite 002:001 intensity ratio (Figure 7) together suggest the development of Al- and/or Fe-hydroxy interlayers in the smectite (Walker, 1961).

CONCLUDING REMARKS

This study illustrates the usefulness of casting bulk chemical data in the form of a reaction progress diagram. Such diagrams more clearly reveal anomalies that might not be noticed, and they thereby tend to stimulate hypotheses that might not otherwise come to mind. This particular study is of interest because it illustrates the importance of oxidation-reduction reactions in clay mineral genesis in a way that is not apparent in other studies. This study also shows that even under conditions of strong leaching it is possible for smectite to form in preference to kaolinite or gibbsite. Finally, in conjunction with the earlier study of the granite saprolite by Gardner *et al.* (1978) it can be seen that rock type has a profound influence on the geochemistry and mineralogy of weathering profiles even in advanced stages of weathering under otherwise homogeneous conditions. In this respect the work corroborates a similar conclusion reached by Clemency (1976, 1977) in a study of the simultaneous weathering of a granite gneiss and an intrusive amphibolite dike near São Paulo, Brazil.

ACKNOWLEDGMENTS

We wish to thank W. G. Leo, M. Pavich, and B. W. Nelson for their helpful reviews. Joyce Goodwin graciously typed several versions of the manuscript.

REFERENCES

Clemency, C. V. (1976) Simultaneous weathering of a granitic gneiss and an intrusive amphibolite dike near Sao Paulo, Brazil, and the origin of clay minerals: *Proc. Int. Clay Conf., Mexico City, 1975,* S. W. Bailey, ed., Applied Publishing Ltd., Wilmette, Illinois, 15–25.

Clemency, C. V. (1977) A quantitative geochemical, mineralogical and physical study of some selected rock weathering profiles from Brazil: Rept. to U.S. Army Research Office, State Univ. New York, Buffalo, 122 pp.

Gardner, L. R., Kheoruenromne, I., and Chen, H. S. (1978) Isovolumetric geochemical investigation of a buried granite saprolite near Columbia, S.C.: *Geochim. Cosmochim. Acta* **42,** 417–424.

Gardner, L. R. and Kheoruenromne, I. (1980) Siderite veins in saprolite, Cayce, S.C.: *S.C. Div. Geol. Geol. Notes* **24,** 29–31.

Helgeson, H. C., Garrels, R. M., and MacKenzie, F. T. (1969) Evaluation of irreversible reactions in geochemical processes involving minerals and aqueous solutions—II. Applicatons: *Geochim. Cosmochim. Acta* **33,** 455–481.

Jackson, M. L. (1956) *Soil Chemical Analysis—Advanced Course:* 2nd printing, 1965, published by author, Dept. Soil Science, Univ. Wisconsin, Madison, Wisc., 991 pp.

Medlin, J. H., Sinha, N. H., and Bodkin, J. B. (1969) Atomic absorption analysis of silicates employing $LiBO_2$ fusion: *At. Absorption Newlett.* **8,** 25–29.

Millot, G. and Bonifas, M. (1955) Transformations isovolu-

métriques dans les phénomènes de latéritisation et de bauxitisation: *Bull. Serv. Carte Geol. Alsace Lorraine* **8**, 3–30.

Shapiro, L. and Brannock, W. W. (1962) Rapid analysis of silicate, carbonate and phosphate rocks: *U.S. Geol. Surv. Bull.* **1144-A**, 56 pp.

Walker, G. F. (1961) Vermiculite minerals: in *The X-ray Identification and Crystal Structures of Clay Minerals*, G. Brown, ed., Mineralogical Society, London, 297–324.

(Received 28 July 1980; accepted 23 January 1981)

Резюме—Диаграммы прогресса эмпирических реакций, демонстрируюшие тенденции концентраций элементарных окисей (г/см^3) как функции основной плотности для диабазового сапролита, показали нарушение непрерывности тенденции Al_2O_3, MgO, H_2O^+, и неэкстрагирующегося Fe_2O_3. Это нарушение непрерывности соответствует нарушению непрерывности тенденции (1) соотношения интенсивности пика 001 каолинита-смектита, (2) соотношения интенсивности пиков 002-001 смектита, и (3) основного расстояния смектита как функции плотности. Эти нарушения непрерывности связаны, очевидно, с условиями восстановления-окисления в профиле выветривания, так как они выступают на глубине, на которой в сапролите первый раз появляются жилы сидерита. Условия окисления в верхней части профиля показывают, что формирование смектита богатого Fe, более вероятно, чем формировение каолинита, в то время как условия восстановления на большой глубине в профиле способствовали формированию каолинита более, чем смектита богатого Al. Эти результаты показывают, что если геохимические условия способствуют сохранению Fe более, чем Al, формирование смектита является предпочтительнее, чем формирование каолинита или гиббсита, даже в условиях сильного выщелачивания. [E.C.]

Resümee—Empirische Reaktionsdiagramme, die die Trends der Hauptelementkonzentrationen (in g/cm^3) in Abhängigkeit von der Durchschnittsdichte eines Diabassaproliten darstellen, zeigen Diskontinuitäten in den Trends von Al_2O_3, MgO, H_2O+, und nichtextrahierbarem Fe_2O_3. Diese Diskontinuitäten fallen mit denen in den folgenden Trends zusammen: (1) 001-Peakintensitätsverhältnis von Kaolinit und Smektit, (2) 002/001-Peakintensitätsverhältnis von Smektit, (3) Basisabstand des Smektits als Funktion der Durchschnittsdichte. Diese Diskontinuitäten hängen offensichtlich mit den Redox-Bedingungen im Verwitterungsprofil zusammen, da sie in einer Teife auftreten, in der zum ersten Mal Siderit-Adern im Saprolit auftreten. Oxidierende Bedingungen im oberen Teil des Profils scheinen die Bildung von Fe-reichem Smektit gegenüber Kaolinit begünstigt zu haben, während reduzierende Bedingungen in den tieferen Teilen des Profils die Bildung von Kaolinit gegenüber Al-reichem Smektit förderten. Dieses Ergebnis deutet darauf hin, daß dort, wo die geochemischen Bedingungen Fe mehr zurückhalten als Al, Smektite gegenüber Kaolinit und Gibbsit bevorzugt gebildet wird, selbst bei Bedingungen mit starker Auslaugung. [U.W.]

Résumé—Des diagrammes empiriques de progrès de réactions montrent les tendances de concentrations majeures de l'élément oxide (en g/cm^3) en tant que fonctions de densité de masse pour une saprolite diabase révèlent des discontinuités dans les tendances d'Al_2O_3, MgO, H_2O+, et de Fe_2O_3 qui ne peut être extrait. Les discontinuités coincident avec des discontinuités dans les tendances de (1) la proportion d'intensité de sommet kaolinite-smectite 001, (2) la proportion d'intensité de sommet smectite 002-001, et (3) l'espacement de base de la smectite, en tant que fonctions de la densité de masse. Ces discontinuités sont apparemment apparentées à des conditions redox dans le profil d'altération, parcequ'elles se trouvent à une profondeur où les veines de sidérite apparaissent pour la première fois dans la saprolite. Des conditions oxydantes dans la partie supérieure du profil semblent avoir favorisé la formation de smectite riche en Fe aux dépens de la kaolinite, alors que des conditions réduisantes plus bas dans le profil ont favorisé la formation de kaolinite aux dépens de la smectite riche en Al. Ces résultats indiquent qu'où les conditions géochimiques favorisent la rétention de Fe aux dépens d'Al, des smectites peuvent etre formées en préference à la kaolinite ou à la gibbsite, même sous des conditions de lessivage sévère. [D.J.]